Marine Pollution Bulletin 167 (2021) 112285

Contents lists available at ScienceDirect

Marine Pollution Bulletin

journal homepage: www.elsevier.com/locate/marpolbul

Long term simulations of potential oil spills around Cuba

Lars Robert Hole [a,*], Victor de Aguiar [a,f], Knut-Frode Dagestad [a], Vassiliki H. Kourafalou [b], Yannis Androulidakis [a,b], Heesook Kang [b], Matthieu Le Hénaff [c,d], Amilcar Calzada [e]

[a] Norwegian Meteorological Institute, Allegt. 70, 5007 Bergen, Norway
[b] Rosenstiel School of Marine and Atmospheric Science, University of Miami, Miami, FL 33149, USA
[c] Cooperative Institute for Marine and Atmospheric Studies, University of Miami, Miami, FL 33149, USA
[d] NOAA Atlantic Oceanographic and Meteorological Laboratory, Miami, FL 33149, USA
[e] Cuba Institute of Meteorology, La Habana, Cuba
[f] Geophysical Institute, University of Bergen, Bergen, Norway

ARTICLE INFO

Keywords:
Oil spill
Cuba
HYCOM
OpenDrift
Eddies
Stranding

ABSTRACT

Simulations over eight years of continuous surface oil spills around Cuba are carried out to identify the most likely stranding (beaching) locations. The open source Lagrangian oil drift model OpenOil is applied with high resolution hydrodynamic forcing. The actual fraction of the released oil mass reaching different regions is calculated, revealing small differences between a light and a heavy crude oil type. Similar stranding rates for the two oil types are found. Another important conclusion is that, due to the high temporal variability in stranding rates, short term simulations of a few weeks are not suitable to assess environmental risk. The highest stranding rates are simulated in winter in Northern Cuba. It is also found that oil could reach Northern Cuba, Yucatan or Florida in about 3–5 days after a spill.

1. Introduction

This study is motivated by recent advances in the understanding of the role that mesoscale oceanographic processes and air-sea interactions in the southeastern Gulf of Mexico (GoM) may play in the basin-wide transport of hydrocarbons. Although the northern region is the major oil exploration area of the GoM, potential offshore drilling sites were recently identified over the southeastern GoM, especially over the northern, western and southwestern parts of the Cuba's Exclusive Economic Zone (CEEZ; Genaw (2010)), see Fig. 1.

Loop Current (LC) variability, which largely impacts transport processes in the GoM, is closely connected to the release of anticyclonic rings, so-called "Loop Current Eddies". Despite great advances in the understanding of GoM dynamics, parts of the southeastern GoM have not received much attention. This particularly applies to GoM waters off northwestern Cuba, at the core of the LC, due to lack of accessible in situ observational studies in Cuban waters. In addition, this is an area of oil exploration with ongoing activities in Cuban waters. There have been few studies addressing connectivity between the Cuban shelf and the general GoM region.

Lindeman et al. (2001) discussed different transport scenarios and showed how ocean eddies cause retention of larvae on the southwestern Cuban shelf under certain circumstances. Ji et al. (2016) used the OSRA model to estimate the risk patterns due to projected oil and gas development in the GOM outer U.S. continental shelf by modeling over 40 million hypothetical oil spill trajectories over extended areas of the U.S. continental shelf. We have recently identified novel processes inside the Straits of Florida that are related to the LC variability. These include the evolution of mesoscale eddies (Kourafalou et al., 2017) and wind-induced upwelling (Le Hénaff et al., 2020; Androulidakis et al., 2020a), over northwestern Cuba, resulting in strong temperature fronts. The variability (position, strength and volume) of the Florida Current (FC), which is the extension of the LC inside the Straits of Florida, has been found to be strongly related to the mesoscale dynamics that prevail in the northern (Kourafalou and Kang, 2012; Kourafalou et al., 2017; Androulidakis et al., 2020a) and southern (Kourafalou et al., 2017) parts of the Straits. Mesoscale processes around the Yucatan Channel also interact with the LC system variability and thus affect connectivity pathways between the Caribbean Sea and the GoM (Oey et al., 2005). The connection of these processes to the overall LC variability and

* Corresponding author.
E-mail addresses: lrh@met.no (L.R. Hole), victorm@met.no (V. de Aguiar), knutfd@met.no (K.-F. Dagestad), vkourafalou@miami.edu (V.H. Kourafalou), iandroulidakis@rsmas.miami.edu (Y. Androulidakis), hkang@rsmas.miami.edu (H. Kang), mlehenaff@rsmas.miami.edu (M. Le Hénaff).

https://doi.org/10.1016/j.marpolbul.2021.112285
Received 2 July 2020; Received in revised form 5 March 2021; Accepted 11 March 2021
Available online 31 March 2021

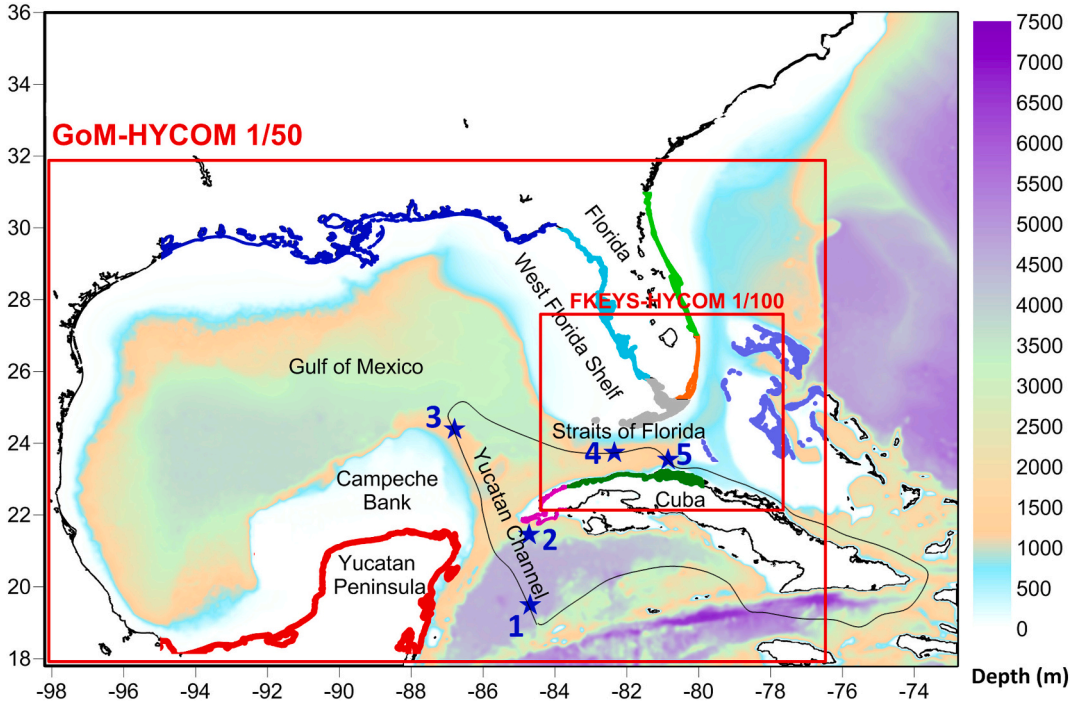

Fig. 1. The coastal regions discussed in this manuscript. Orange = Southeast Florida, Grey = Southwest Florida, Light Green = East Florida, Aqua = West Florida, Dark Green = Northern Cuba, Magenta = Western Cuba, Light Blue = Western Bahamas, Dark Blue: Northern Gulf, Red = Yucatan. The blue stars are oil exploration sites north and west of Cuba in the Cuban Exclusive Economic Zone, CEEZ. CEEZ is shown as a thin solid line. Model domains of the GoM-HYCOM 1/50 and the FKEYS-HYOM 1/100 are embedded in addition to bathymetry (m). (For interpretation of the references to colour in this figure legend, the reader is referred to the web version of this article.)

especially to hydrocarbon pathways has not been previously studied in detail. Although we focus on hydrocarbon transport, datasets with trajectory calculations and their statistics will be useful to a variety of studies of basin-wide GoM connectivity, which have recently found that the understanding of processes near northwestern Cuba is important (Androulidakis et al., 2020b).

Drouin et al. (2019) used a Lagrangian floating oil trajectory model to explore the oil pathways only inside the Straits of Florida. The drift was initiated at locations representative of exploratory drilling sites around CEEZ and their model was integrated for ten days. The simulations exhibited a strong seasonal dependence, where the Florida coast is mostly affected during the summer, and the Cuban coast in the winter. They showed that a significant amount of oil (1–5%) reaches the Florida coastline within two to ten days, and that Cuba is potentially affected within hours. Murawski et al. (2019) tested a blowout scenario similar to the flow rate and period (spring to autumn of 2010) of the Deepwater Horizon (DwH) accident from a site at the western entrance of the Straits of Florida. Results about the effects of the ocean dynamics inside the Straits of Florida on hydrocarbons pathways are discussed by Androulidakis et al. (2020b). These previous studies mainly focused on the circulation effects on oil pathways without discussing in detail decay of oil mass during transport, evaporation, emulsification, vertical mixing and natural dispersion by wave breaking. In addition to including these effects, our approach also takes into account oil releases in several sites around Cuba, covering a large area of the CEEZ at the north (along the Straits of Florida), west (Yucatan Channel), northwest (inner Gulf) and southwest (northern Caribbean Sea) of the island (Fig. 1). We also expand the previous studies by computing the possibility of stranding at the entire Gulf and adjacent Atlantic coasts of Florida and the Bahamas.

Here, we address the following research questions: 1. What are the main oil pathways in the vicinity of the LC system in the GoM area? 2. How likely is it that an oil spill from any of the Cuban exploration sites would reach the shore? 3. How large fraction of the spilled oil mass could eventually reach different regions such as Cuba, Yucatan, Florida, and the Bahamas?

We use a combination of high resolution ocean models and an up to date Lagrangian oil transport model to calculate drift and weathering over 8 years from continuous oil spills at selected locations in the CEEZ, see Fig. 1. We focus on seasonal and spatial variations. Here we present results from five representative points (1–5 in clockwise direction for the sake of clarity). The datasets produced are open and available online.

2. Methods

2.1. Metocean forcing

The main ocean circulation fields for this study were derived from a data-assimilative, high- resolution (1/50°, 1.8 km) configuration of the Hybrid Coordinate Ocean Model (HYCOM, 2020) in the GoM, developed by the authors (GoM-HYCOM 1/50, Fig. 1). GoM-HYCOM 1/50 uses daily river forcing and data assimilation. The HYCOM model has a flexible, hybrid vertical coordinate system, in which the distribution of vertical layers is optimized: they are isopycnal in stratified water columns, terrain- following sigma in regions with sharp topography, and isobaric in the mixed layer and very shallow areas (Bleck, 2002). More information about HYCOM is available in the model user's manual ((HYCOM, 2020) and references therein). The GoM-HYCOM 1/50 covers the entire GoM, the northern Caribbean Sea and the adjacent Atlantic areas between Florida and Bahamas, and uses 32 vertical layers. This model configuration is similar to the one used by Le Hénaff and Kourafalou (2016), with the realistic river forcing parameterization developed by Schiller and Kourafalou (2010). The river discharge data were obtained from the Army Corps of Engineers and the U.S. Geological Survey. The model is initialized in October 2009 with fields from the operational GLoBal HYCOM simulation run at the Naval Research Laboratory at the Stennis Space Center (GLB-HYCOM expt90.8, (HYCOM, 2020)), and it is nested at the open boundaries with model fields from the same global simulation. The atmospheric forcing is based on the

Table 1
Summary of metocean forcing used in the oil drift simulations. GoM-HYCOM 1/50 was 3 hourly for 2010, and daily for the rest of the period. See also Fig. 1.

Model		Resolution:		
Model	Parameters	Horizontal	Vertical	Temporal
GoM-HYCOM 1/50	Surface current	1/50°	32 layers	Daily
FKEYS-HYCOM 1/100	Surface current	1/100°	26 layers	6 h
ECMWF atmospheric model	Wind velocity, air temperature	1/8°	Surface	3 h
ECMWF wave model	Stokes drift, wave height and period	1/8°	Surface	12 h

three-hourly winds, thermal forcing and precipitation forecast fields from the European Centre for Medium-Range Weather Forecasts (ECMWF, 2020), with spatial resolution of 0.125° (see below). The ECMWF provides daily global forecasts at 0:00 and 12:00 UTC with 0.125° resolution. Recent model upgrades have improved the overall performance of the forecasting system throughout the medium range. Further details on the ECMWF model description and verification can be found e.g., in the works of Ehard et al. (2016) and Haiden et al. (2016), and at ECMWF (2020). In this study, ECMWF daily forecast products were also used to provide air temperature and wind drag for the OpenOil simulations with a 3 hourly time step.

GoM-HYCOM 1/50 assimilates satellite fields of Sea Surface Temperature and Sea Surface Height, and in situ observations of temperature and salinity from buoys, cruises, surface drifters, Argo floats and XBT casts. More details about the model configuration can be found in Le Hénaff and Kourafalou (2016); Androulidakis et al. (2019, 2021). We used a detailed treatment of plume dynamics in HYCOM, based on Schiller and Kourafalou (2010) that builds on a widely used parameterization that includes both salinity and momentum fluxes, pioneered by Kourafalou et al. (1996). Androulidakis et al. (2019) showed the realism of the GoM-HYCOM 1/50 simulation on river plume spreading, with good agreement between model and observations (satellite and in situ). Hole et al. (2019) also used the GoM-HYCOM 1/50 ocean forcing data of OpenOil simulations, and obtained excellent agreement with satellite observations of the DeepWater Horizon oil slick. The good performance of GoM-HYCOM 1/50 in the Straits of Florida is confirmed by Androulidakis et al. (2020a) who used the model to describe the role of eddies and upwelling near Cuba on the Gulf Stream evolution.

To increase the resolution over the northern CEEZ a higher resolution (1/100° or 900 m) model, developed over the Florida Straits, South Florida and the Florida Keys (FKEYS-HYCOM; Kourafalou and Kang, 2012) was also used to force the oil drift simulations. The model includes all South Florida coastal and shelf areas and extends across the Straits of Florida to Cuba and the Bahamas (Fig. 1). The domain is chosen to ensure the proper representations of the complex South Florida coastal system, and accommodate the influence of the strong LC/FC system and associated eddies. The FKEYS-HYCOM simulation does not assimilate observations directly, but it is nested in the GoM-HYCOM 1/50, which ensures that it is forced with realistic currents and eddy field. FKEYS-HYCOM 1/100 also uses ECMWF atmospheric forcing described above.

Wave properties were acquired from the ECMWF third generation spectral WAve Model (WAM) global operational runs (ECMWFwave, 2020). The WAM model (e.g. (Group, 1988; Haiden et al., 2016)) computes a two-dimensional wave distribution, with 25 frequencies and 24 directions. The operational WAM forecasts used here are also forced by the ECMWF forecasts. The wave output with 0.125° horizontal resolution was downloaded with 12-hourly time step and used here for calculating horizontal Stokes drift and vertical mixing of the oil with a three-hourly time step using linear interpolation in time. From the two-dimensional wave spectra, the surface Stokes drift, significant wave height, and mean wave period were computed and used in the oil drift model for the calculation of wave-induced transport and mixing. For the wave-induced transport, a vertical Stokes drift profile is computed based on surface Stokes drift, significant wave height and mean wave period according to Breivik et al. (2016). The various forcing data are summarized in Table 1.

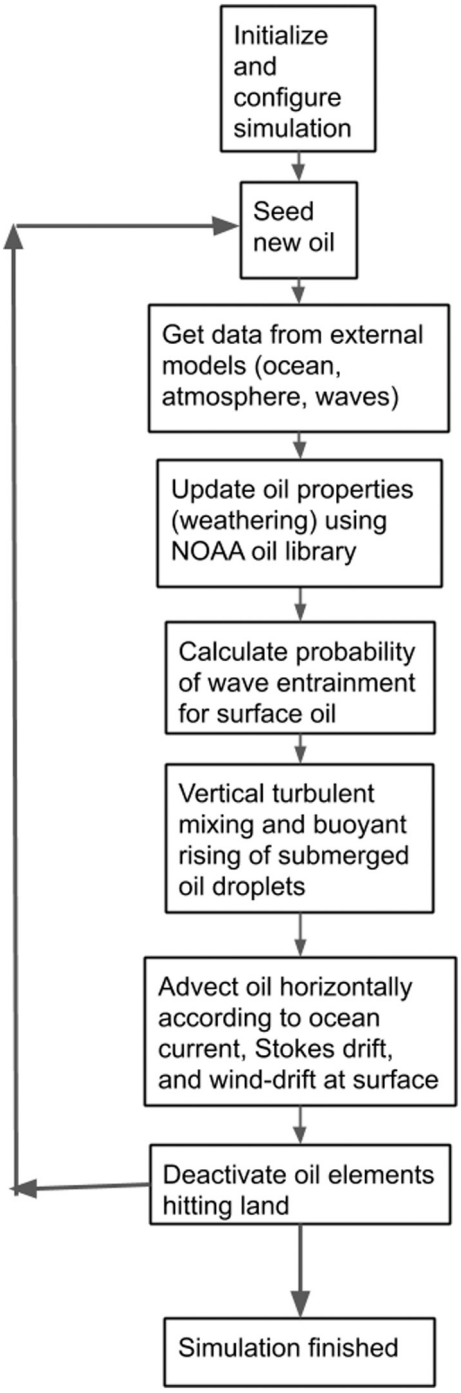

Fig. 2. Flow chart showing the sequence of operations involved in the OpenOil simulations.

2.2. The oil drift model OpenOil

OpenOil is part of the OpenDrift trajectory modeling framework (Dagestad et al., 2018), developed at the Norwegian Meteorological Institute and available as open source software from OpenDrift (2020). OpenOil has been evaluated against drifter and oil slick observations in

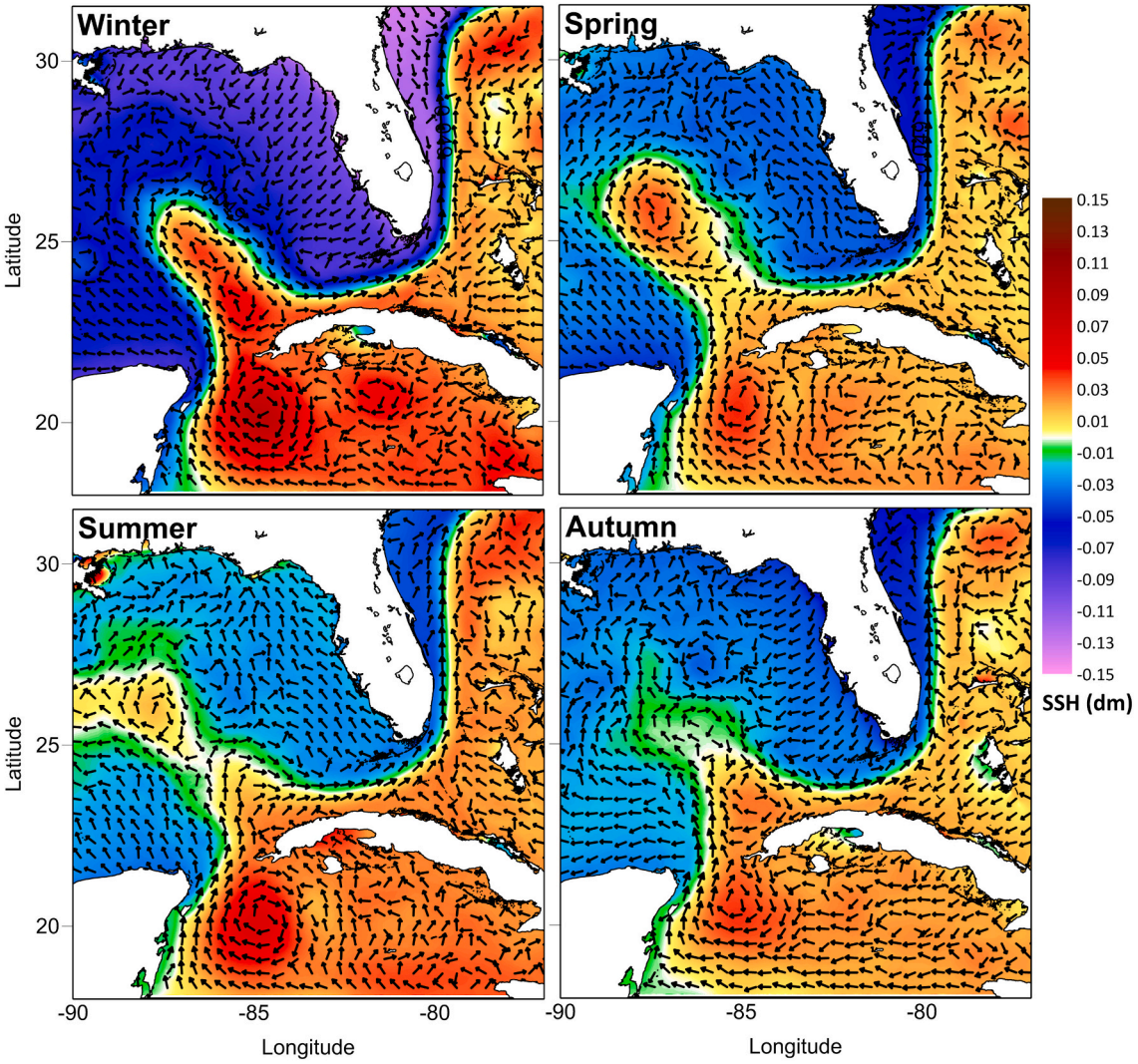

Fig. 3. Seasonal Sea Surface Height (SSH) in dm (colour) and surface currents (vectors) from the GoM-HYCOM 1/50 model, 2010–2017. (For interpretation of the references to colour in this figure legend, the reader is referred to the web version of this article.)

the North Sea (Jones et al., 2016; Röhrs et al., 2018; Dagestad and Röhrs, 2019) and good correspondence has been found when using an empirical wind drift factor of 2% for surface oil, in addition to the Stokes drift and ocean currents. A similar wind drift factor is used in other oil spill trajectory modeling in GoM (Abascal et al., 2015). Details of the element tracking model are given in Dagestad et al. (2018), and model physics that are specific to oil transport and fate are documented in Röhrs et al. (2018) and in the following paragraphs.

OpenOil is an integrated oil drift model consisting of sub-models for specific physical processes such as wave entrainment of oil (Li et al., 2017c), vertical mixing due to oceanic turbulence and waves (Nordam et al., 2019; Röhrs et al., 2018), resurfacing of oil due to buoyancy (Tkalich and Chan, 2002), and emulsification and evaporation taking into account oil properties (Lehr et al., 2002). The resurfacing is a function of oil density and droplet size following Stokes Law, and thereby the model physics are very sensitive to the specification of the oil's droplet size. Fig. 2 shows the sequence of operations involved in the OpenOil simulations. Openoil has recently been used in the GoM to simulate both the DwH oil spill (Hole et al., 2019) and the effects of ocean dynamics on hydrocarbon transport in the Straits of Florida (Androulidakis et al., 2020b). OpenOil has recently been shown to provide excellent agreement with free floating oil drift in the open ocean as verified against remote sensing observations in the North Sea by Brekke et al. (2020).

2.3. Oil droplet size distribution

Several algorithms are implemented in OpenOil to describe the droplet size distribution of entrained oil. Here, we use the size distribution based on Li et al. (2017b). Hole et al. (2019) showed that the net result was almost indistinguishable from the classical distribution provided by Delvigne and Sweeney (1988) for week-long simulations of the DwH oil slick. Li et al. (2017b) takes the oil viscosity and the oil–water interfacial tension into account. This parameterization describes a log-normal law for the number size distribution (number of droplets per size class), and the resulting volume size distribution exhibits a peak at an intermediate droplet size of about 100 μm, depending on oil type and environmental conditions. Similar types of droplet size distribution have been developed and observed, confirming that there is a maximum in oil volume at a particular droplet size (Johansen et al., 2015; Li et al., 2017a).

Following Li et al. (2017b), the volume (V) droplet size spectrum is described by the median droplet diameter, D_{50}^{V}, as

$$D_{50}^{V} = d_o r(1 + 10\mathrm{Oh})^{p} \cdot \mathrm{We}^{q} \quad (1)$$

with the empirical coefficient r=1.791 and the exponents p=0.460 and $q = -0.518$. The droplet size distribution follows a log-normal distribution around the medium diameter with a logarithmic base-10

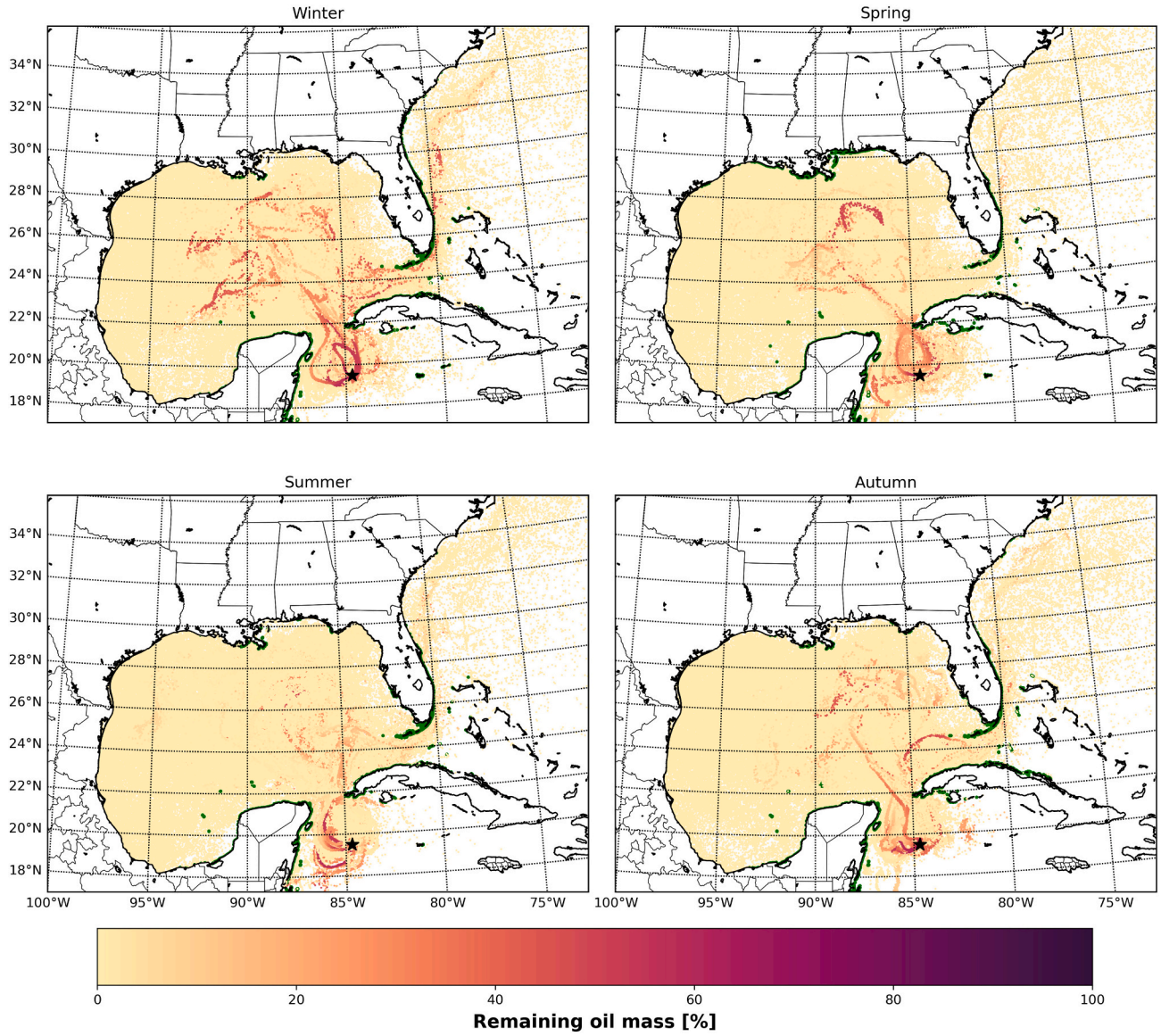

Fig. 4. Seasonal patterns of remaining mass of oil for the continuous surface oil spill 2010–2017, point 1 (black star), light oil. The figure shows all monthly element locations during the simulation period and oil elements are coloured by remaining oil mass percentage (residual) relative to initial mass. Winter is defined as December–February, spring is March–May, summer is June–August and autumn is September–November. Green areas indicate stranded oil elements. (For interpretation of the references to colour in this figure legend, the reader is referred to the web version of this article.)

standard deviation of s=0.38 (Eq. 16 in Röhrs et al. (2018)). The Ohnesorge number (Oh) and Weber number (We) are further defined in the appendix.

Droplet sizes are assigned to oil particles each time an element is submerged by breaking waves, following the wave entrainment algorithm of Li et al. (2017c). The implementation of this algorithm in OpenOil is described with full detail in Röhrs et al. (2018). The droplet sizes for individual particles are drawn from a random distribution according to the chosen size distribution. The size distributions represent conditions for a stochastic wave entrainment event, representing equilibrium conditions during a model time step. The overall size distribution of all submerged oil in the simulation is further subject to changes, as weather conditions, the oil's emulsification rate change and oil droplets of various sizes are subjected to various resurfacing time scales. Resurfaced elements are considered to be part of a surface slick, and are assigned a new droplet size distribution once they are re-entrained. Oil droplets at the sea surface (slick) are not considered to have a radius.

2.4. Horizontal transport

With regard to horizontal drift, three processes are considered: currents, Stokes drift and wind drift. Any element, whether submerged or at the surface, drifts along with the ocean current. Elements are further subject to Stokes drift corresponding to their actual depth. Surface Stokes drift is normally obtained from a wave model, and its decrease with depth is calculated as described in Breivik et al. (2016). Oil elements at the ocean surface are additionally advected with a factor of 2% of the wind. Together with the Stokes drift (typically 1.5% of the wind at the surface), it sums up to the commonly found empirical value of 3.5% of the wind speed (Schwartzberg, 1971). The magnitude of the wind drift factor was discussed by Jones et al. (2016) who stated that a 2% wind drift factor was required in OpenOil to reproduce their observations of a surface oil patch in the North Sea. Brekke et al. (2020) also found excellent agreement with observed spills in open ocean by applying the same wind drift factor and Stokes drift formulation in OpenOil. In essence, the wind drift is believed to be a compensation

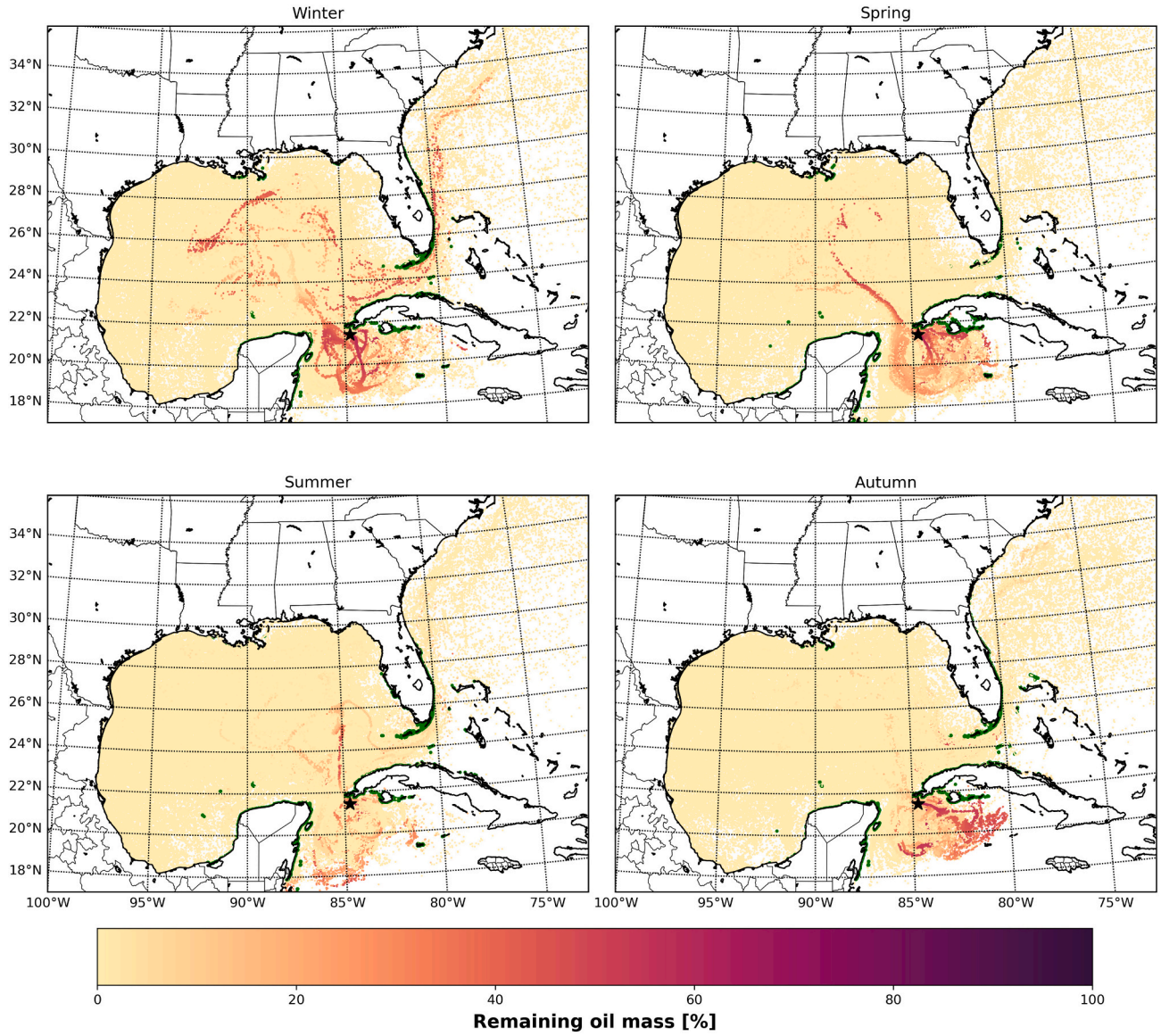

Fig. 5. Same as Fig. 4, but for point 2.

factor for the inability of any ocean model to represent the strong shear current in the upper few centimeters/decimeters of the ocean, and not due to surface oil actually moving relative to the water. Wind drift was found to be important in bringing the oil to the northern Gulf beaches (Liu et al., 2011; Le Hénaff et al., 2012; Weisberg et al., 2017; Hole et al., 2019).

The three horizontal drift components (currents, Stokes drift and wind drift) may lead to a very strong gradient of drift magnitude and direction in the upper few meters of the ocean. For this reason, it is also of critical importance to have a good description of the vertical oil transport processes.

2.5. Vertical transport

Oil elements at the surface, regarded as being in the state of an oil slick, may be entrained into the ocean by breaking waves. The entrainment of oil droplets depends on both the wind and wave (breaking) conditions, but also on the oil properties, such as viscosity, density and oil–water interfacial tension. The buoyancy of droplets is calculated according to empirical relationships and the Stokes law following Tkalich and Chan (2002), depending on ocean stratification based on temperature and salinity from the ocean model, and the viscosities and densities of oil and water.

In addition to the wave induced entrainment, the oil elements are also subjected to vertical turbulence throughout the water column, described using a random-walk scheme of Visser (1997) with turbulent eddy diffusivity parameterized from wind speed according to Sundby (1983).

2.6. Oil weathering

To calculate weathering of the oil, OpenOil interfaces with the open source ADIOS oil library (NOAA-Oil, 2020), developed by NOAA (Lehr et al., 2002). In addition to state-of-the-art parameterization of weathering processes such as evaporation, emulsification and dispersion, this software contains a database of measured properties of almost 1000 oil types from around the world. As oils from different sources or wells have vastly different properties, such a database is of vital importance for accurate results. The ADIOS oil library is also used by the NOAA oil drift model PyGnome (oildrift, 2019).

The weathering algorithms describes evaporation and emulsification rate of oil, i.e., the water content. The emulsification and evaporation

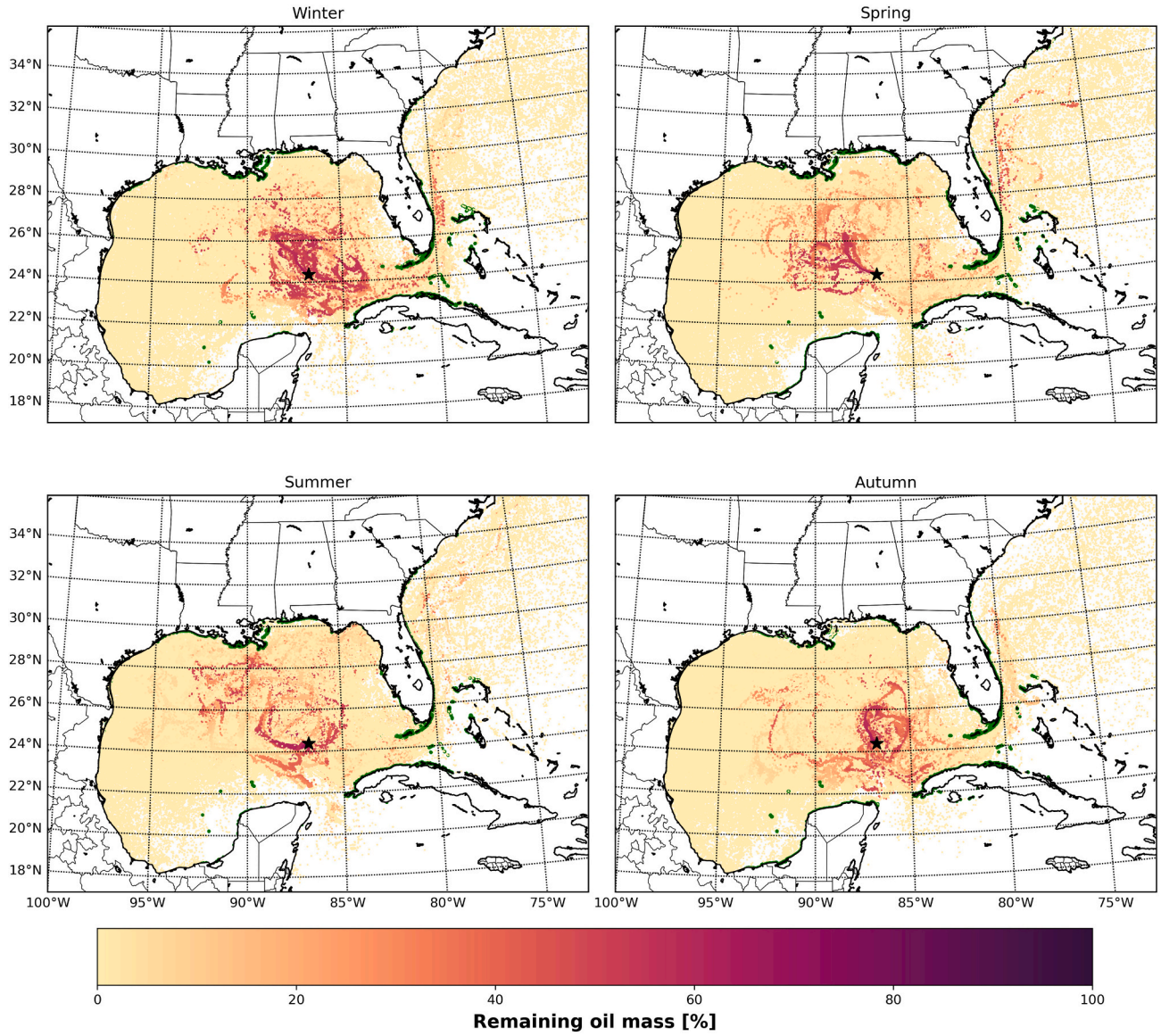

Fig. 6. Same as Fig. 4, but for point 3.

greatly affect oil density, viscosity and oil–water interfacial tension, and thereby the droplet size distribution through Eqs. (1)–(3).

2.7. Experimental design

OpenOil (part of the OpenDrift framework v1.5.3) was run with a 1 hourly time step. In the present study, we released 100 oil elements daily during the 2010–2017 period (eight years) for 5 potential drilling locations in the CEEZ Fig. 1. We conducted the simulations with two types of oil: the Light Louisiana Sweet (34.8°API) oil type from the NOAA ADIOS Oil database was used as well as the heavier IFO-180LS 2014 (13.2°API), hereafter referred to as *light* and *heavy* respectively. The light oil will emulsify quickly after release, while the heavy oil does not emulsify. The total number of the simulations performed for this study is 10 (5 release sites × 2 oil types, altogether 80 years). Stranded oil mass was calculated for different coastal regions (Fig. 1). Here, oil elements are considered stranded when they hit the coastline. The Global Self-consistent, Hierarchical, High-resolution Shoreline Database (GSHHS) was used to define the coastline. While continuous oil spills over eight years are obviously not realistic, this type of simulation is valuable for statistical purposes. It has provided the necessary scenarios of pathways under a highly variable dynamical current system to provide a statistical impression on the most probable pathways, transport times to shore and stranding locations for spills in the CEEZ.

3. Results

Fig. 3 presents the mean seasonal circulation patterns of the Gulf derived from the GoM-HYCOM 1/50 simulations during the entire 2010–2017 period. The LC is extended northwestward during winter (December–February) and spring (March–May), while retracted LCs over the southeastern Gulf prevails during autumn (September–November). In summer (June–August), the LC itself is retracted and a newly detached LC Eddy appears present just north of it. Differences in the seasonal circulation are also detected south of Yucatan Channel with very strong and large anticyclonic eddies especially in winter and summer. The ocean dynamics and especially the LC evolution which is the main circulation feature in the GoM (Sturges and Evans, 1983) determine the connectivity in the the Gulf (Schiller and Kourafalou, 2010; Le Hénaff and Kourafalou, 2016; Androulidakis et al., 2019) and thus control the evolution of oil pathways (Androulidakis et al., 2020b). Androulidakis et al. (2020b), based on an inter-annual analysis, showed

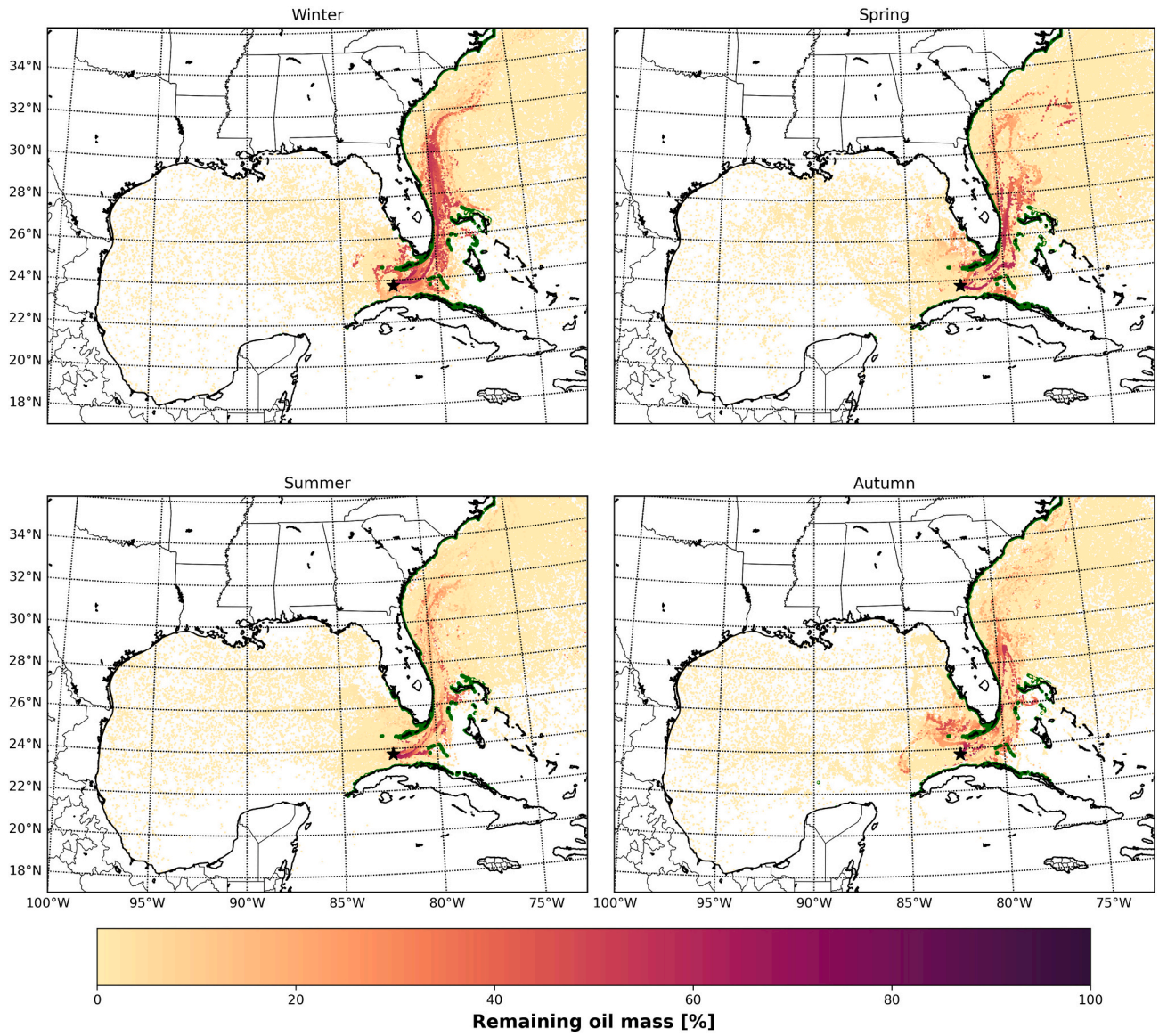

Fig. 7. Same as Fig. 4, but for point 4.

that the regional and local ocean dynamics are significant indicators to predict the oil fate and stranding along the Gulf's coasts. Herein, we present results for selected simulations at certain release points that highlight the influence of different aspects of the oceanic seasonal variability both north and south of the Yucatan Channel. We start with releases from south of the Yucatan (points 1 and 2), then the Gulf of Mexico interior (point 3) and finally the Straits of Florida (points 4 and 5).

The formation of strong anticyclonic eddies just south of Yucatan, especially in winter contributes to the increased oil density levels over the same area and especially inside the anticyclones for oil released at point 1 (Fig. 4). In the figure all monthly element locations are shown. In these simulations, the elements will loose mass due to evaporation and natural dispersion by breaking waves. Elements with remaining mass will be days to weeks old, so the elements with remaining mass in the figures illustrate the most efficient pathways from the release points. Similarly, oil from point 2 in summer (Fig. 5) also follows this anticyclonic circulation in the northwestern Caribbean Sea. This pathway is not so evident during other seasons. Pérez-Santos et al. (2015) described a westward counter current along the northern coast of Cuba and its interaction with the anticyclonic vortex south of Yucatan. The Cuban counter current is stronger in summer than in winter and in concert with westward winds it can bring oil into the Yucatan vortex and then northwards by the Yucatan current (Fig. 3). This is probably the reason why little oil, released at point 2, was detected in the inner Gulf (north of the Yucatan Channel) in summer and autumn (Fig. 5), contrary to winter and spring, when a northward pathway of oil from the Yucatan Channel to the central Gulf is evident. Similar findings were derived at point 1 for both light (Fig. 4) and heavy oil (not shown). The influence of the persistent anticyclonic circulation near the release point 2 is evident, similar to the findings for point 1. Again, this results in local retention of elements, which is now enhanced by the proximity of land, as point 2 is close to Cuba. Elements are thus more limited from entering the Yucatan Channel, as compared to those from point 1 that have an easier pathway of entering the Gulf of Mexico.

Next, we present results from the release at point 3, as a characteristic example for releases within the CEEZ at the GoM interior. The limited spreading of oil elements inside the inner GoM (Figs. 6) is associated with the small LC extension in summer and autumn (Fig. 3). The LC is more extended in winter and spring, when oil released at point 3 (Fig. 6) follows the LC along its clockwise curve towards the Straits of Florida. Androulidakis et al. (2020b) showed that the elongated and

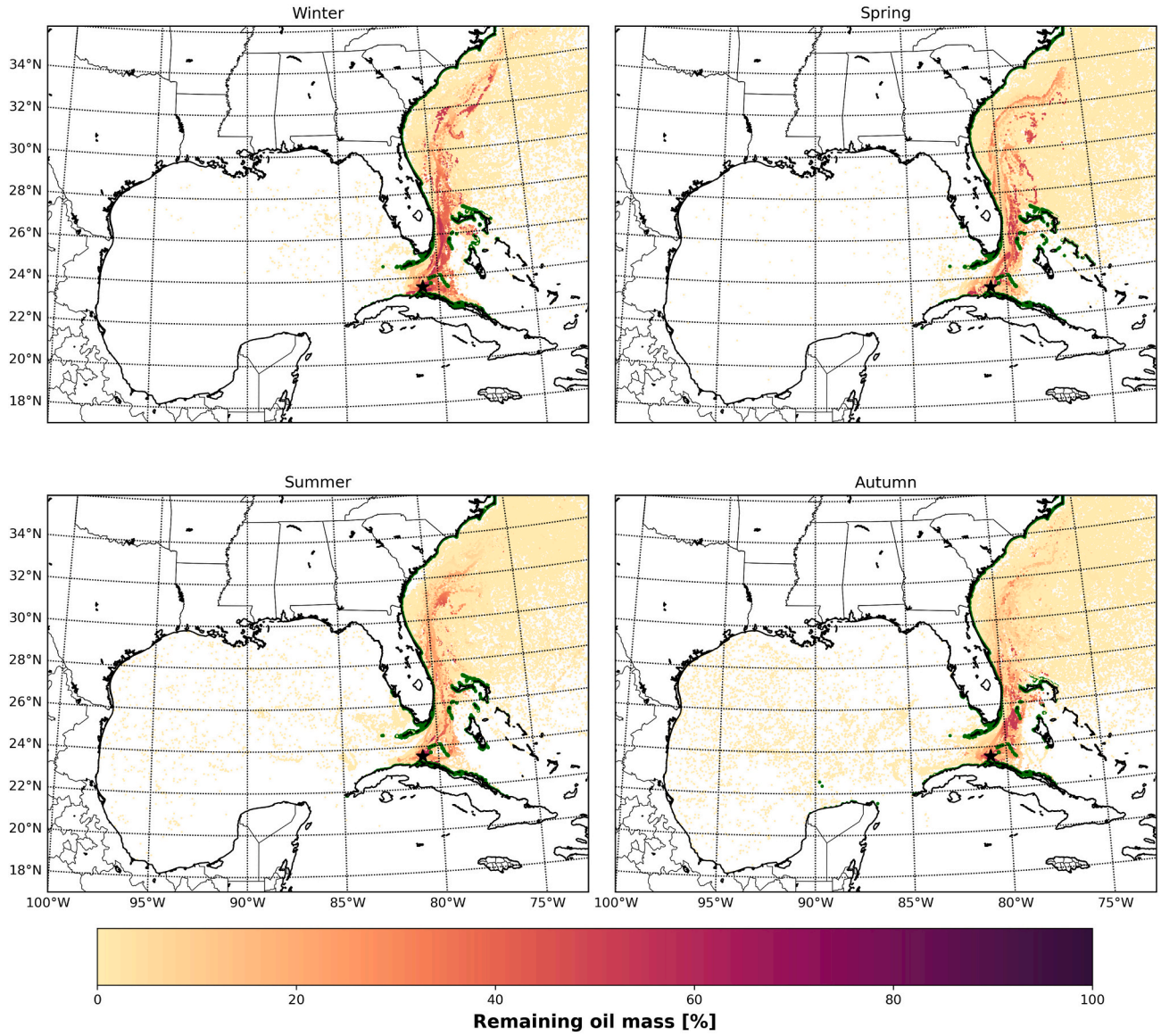

Fig. 8. Same as Fig. 4, but for point 5.

retracted LC phases in relation to the location of the release area may reveal different impacts on the pathways of ocean tracers. In summer and autumn, elements are not dragged by the LC, which usually evolves south of the released point 3 (retracted LC). In addition, oil elements reached their highest latitudes in spring, increasing the oil particle density close to the northern shelves and the Mississippi River Delta (Fig. 6). The retracted LC in summer and autumn agrees with the high oil density north of the LC, when oil is released at point 3; high oil density is aligned with the perimeter of a vortex (eddy) at 26°N indicating the occurrence of anticyclonic eddies such as LC rings (e.g. Oey et al. (2005)) or Western Florida Anticyclones (WFAs; Kourafalou et al. (2018)) that usually evolve over this area during the retracted LC phases.

The seasonal distribution of the remaining oil mass released at point 4 is presented in Fig. 7. The majority of oil was detected inside the Straits of Florida, while only small quantities were spread inside the inner Gulf. A direct eastward jet of oil with weak spreading towards the northern Cuban coast was identified in autumn. The retracted LC phases that prevailed during autumn are generally related to extended FC phases, reaching the northern part of the Straits (Androulidakis et al., 2020a) where point 4 is located. On the contrary, the extended LC phases are associated with FC evolution closer to the Cuban coast (Fig. 3), south of the release point, in agreement with Androulidakis et al. (2020a) findings. During retracted FC phases, closer to Cuba, the circulation over the northern Straits is mainly characterized by cyclonic eddies that evolve along the Florida Keys (Kourafalou and Kang, 2012; Androulidakis et al., 2020a). Oil masses, released from the northern point 4, were entrapped inside these eddies and remained over the northern central Straits (82°W; Fig. 7). Similar results were also derived for spring, when extended LCs also occurred.

Finally, we present results from the release at point 5, as a characteristic example for releases within the CEEZ and close to the northern Cuban coast. Similar to point 4, this release did not result in significant quantities of oil inside the GoM, while the majority of the oil mass followed the eastward transport of the FC towards the Gulf Stream in the Atlantic Ocean (Fig. 8. The north-south variations of the FC affect the fate of pollutants both inside the Straits of Florida and further downstream along the US Atlantic coasts (Androulidakis et al., 2020b). Small seasonal differences inside the GoM were probably related to the different ocean and wind dynamics over the Straits and especially over the West Florida Shelf that control the connectivity from the Straits to the inner Gulf (Androulidakis et al., 2020b); strong westward currents

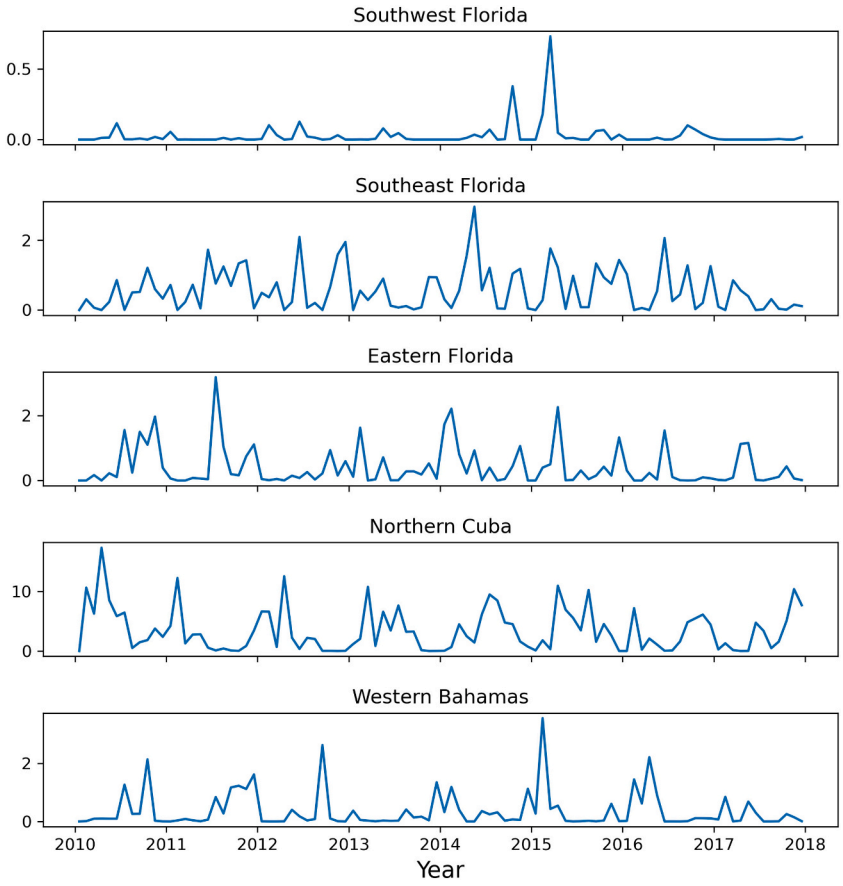

Fig. 9. Monthly percentage of oil to reach different shores (Fig. 1) for oil released at point 5, light oil. Only locations with more than 1% monthly stranding are shown. Note that the vertical scale is different for each location.

Table 2
Percentage of oil mass stranded, percentage of elements stranded and stranding age of oil elements (mean and minimum transport time to shoreline) in selected regions (Fig. 1), for continuous oil spill at point 1 during 2010–2017 (Fig. 4).

Region	Percentage, light oil (%):	Percentage, heavy oil (%):	Elements, (%):	Mean time to shoreline (days):	Minimum time to shoreline (days):
Southwest Florida	0.0	0.1	3.9	62.5	18.4
Southeast Florida	0.1	0.2	3.5	61.2	17.1
Eastern Florida	0.0	0.1	2.2	67.4	15.2
Western Florida	0.0	0.1	2.8	84.5	26.2
Northern Cuba	0.0	0.1	3.5	59.6	15.0
Western Cuba	0.1	0.2	3.4	41.2	7.4
Western Bahamas	0.0	0.0	0.6	113.3	26.0
Northern Gulf	0.0	0.3	16.0	90.9	43.2
Yucatan	0.2	0.6	18.4	40.0	5.1

Table 3
Same as Table 2, but for point 2.

Region	Percentage, light oil (%):	Percentage, heavy oil (%):	Elements, (%):	Mean time to shoreline (days):	Minimum time to shoreline (days):
Southwest Florida	0.0	0.1	4.2	70.2	24.7
Southeast Florida	0.0	0.2	3.6	67.8	26.6
Eastern Florida	0.0	0.0	2.3	73.3	27.4
Western Florida	0.0	0.0	2.3	100.9	40.8
Northern Cuba	0.01	0.1	4.2	60.5	7.8
Western Cuba	1.1	2.2	12.0	32.2	4.4
Western Bahamas	0.0	0.0	0.6	122.8	39.6
Northern Gulf	0.0	0.3	15.2	96.9	47.9
Yucatan	0.0	0.4	15.2	51.1	14.4

Table 4
Same as Table 2, but for point 3.

Region	Percentage, light oil (%):	Percentage, heavy oil (%):	Elements, (%):	Mean time to shoreline (days):	Minimum time to shoreline (days):
Southwest Florida	0.1	0.3	4.7	53.0	16.8
Southeast Florida	0.1	0.3	5.0	55.3	13.25
Eastern Florida	0.0	0.1	2.5	58.4	16.6
Western Florida	0.1	0.2	4.8	77.1	23.2
Northern Cuba	0.1	0.3	5.8	47.9	14.7
Western Cuba	0.0	0.2	2.0	46.4	13.8
Western Bahamas	0.0	0.0	1.1	105.1	13.0
Northern Gulf	0.2	0.7	21.6	81.2	21.7
Yucatan	0.0	0.1	5.3	76.0	26.6

Table 5
Same as Table 2, but for point 4.

Region	Percentage, light oil (%):	Percentage, heavy oil (%):	Elements, (%):	Mean time to shoreline (days):	Minimum time to shoreline (days):
Southwest Florida:	2.5	4.1	22.3	10.8	3.4
Southeast Florida:	3.1	5.1	18.4	10.3	4.2
Eastern Florida:	0.6	1.0	11.1	18.2	4.7
Western Florida:	0.0	0.0	0.8	53.4	6.7
Northern Cuba:	0.3	0.6	6.4	24.0	3.7
Western Cuba:	0.0	0.0	0.3	52.8	8.1
Western Bahamas:	0.2	0.3	4.0	69.5	6.6
Northern Gulf:	0.0	0.0	0.5	126.9	55.6
Yucatan:	0.0	0.0	0.1	113.1	41.7

Table 6
Same as Table 2, but for point 5.

Region	Percentage, light oil (%):	Percentage, heavy oil (%):	Elements, (%):	Mean time to shoreline (days):	Minimum time to shoreline (days):
Southwest Florida:	0.0	0.1	13.0	17.5	3.4
Southeast Florida:	0.5	1.3	2.9	10.0	3.8
Eastern Florida:	0.4	1.4	11.9	18.2	5.4
Western Florida:	0.0	0.0	0.1	53.0	11.7
Northern Cuba:	3.1	9.1	22.5	6.6	2.6
Western Cuba:	0.0	0.0	0.0	45.8	13.4
Western Bahamas:	0.3	12.0	4.5	49.0	9.8
Northern Gulf:	0.0	0.0	0.1	134.8	48.5
Yucatan:	0.0	0.0	0.0	29.7	69.0

related to easterly winds were detected in winter over the West Florida Shelf Fig. 3. The offshore currents over the shelf contributed to the oil mass spreading over the entire GoM in autumn (Fig. 8), in comparison to the other seasons when the oil was mainly restricted to the West Florida shelf.

4. Discussion and conclusions

The stranding rate is highly variable in time (Fig. 9). Tables 2–6 reveal that the fraction of heavy oil reaching the shore is less than 1% on average for most regions, but typically about twice the fraction of light oil in most cases.

Looking at the total load for all regions, for some months about 5% of the released oil mass from point 5 (Fig. 9), a location in the central Straits of Florida near Cuba, could reach the beaches of Florida. About the same fraction of the oil released from point 1 could potentially reach the Yucatan coast (not shown).

The highest stranding rates of oil released at point 5 were computed for the Northern Cuba coastline, where more than 10% of the oil mass reached the coastline during several periods and the standing rate, averaged over the entire period was 3.2 and 6.0% for light and heavy oil, respectively (Table 6). The northern coast of Cuba is mainly affected by oil released close to the shore (e.g. point 5), especially when the FC evolves close to Cuba (Androulidakis et al., 2020b). As presented in Fig. 9, the majority of the oil remained in the eastern Straits and spread in the Atlantic between Florida and the Bahamas along the Gulf Stream. Thus, stranding was mainly identified at the coasts of Florida (Southwest, Southeast, Eastern) and Bahamas (Western). The rest of the Gulf coasts revealed stranding rates well below 1% for all release points (Tables 2–6). It is evident that one must distinguish between the number of Lagrangian elements and the actual oil mass that reach the different shores. For example, the oil released from the westernmost point (point 3, in the Gulf interior, off the northeastern corner of Campeche Bank) will be several weeks to months old when it reaches the Northern Gulf, and even if 21.6% of the elements reach this region, only 0.7% of the released mass will remain (Table 4). Hardly any oil mass released from point 3 will reach the shores. The oil mass distribution pattern in Fig. 6 can be explained in part by the ocean circulation patterns (LC, LC Eddies, cyclonic and anticyclonic eddies), causing efficient transport of oil, and in part by onshore wind. Stranding rates can be presented as fraction of released oil mass instead of fraction of released elements since a large fraction of the mass decays en route to the shore. (Tables 2–6, Fig. 9).

Based on the ten eight-year simulations presented here, only small amounts of oil could statistically reach nearby coastlines from a major oil spill in Cuban waters. Maximum 3% of the monthly released mass of oil from point 5 was found to strand in South Florida (less than 1% of the oil mass on average), see Table 6, in line with the findings of Drouin et al. (2019). However, short-term scenarios might increase this risk. Stranding rates are mostly seasonal in Northern Cuba, particularly for point 5 (which is close to the Cuban coast), revealing the effect of the stronger NE trade winds in winter (Fig. 9). The highly variable stranding rates shown in Fig. 9 suggest that short term simulations over a few weeks can provide misleading conclusions.

The summer simulations are more dispersed than the winter simulations and show large clusters of elements in the Straits of Florida, the Florida Keys, off the South Florida coast, and northwest of the Cuban coast. Variations are seen between the individual spill locations, as coherent vortices have the ability to trap elements and change their distribution. The Bahamas remain largely unaffected, with a small probability of impact predicted for the Western Bahamas. The maximum latitudinal extent of the simulations suggests that oil elements could reach the latitude of the Florida-Georgia border within ten days.

We further note that the behavior of oil elements is strongly dependent on the initial spill location and the initial spill parameters. The large-scale oceanic currents and the wind and wave fields play a dominant role in the distribution of oil at the sea surface (Jones et al., 2016). We have demonstrated that this is particularly true in the study area, where coastal to offshore interactions are intense, extending findings by Weisberg et al. (2017), Androulidakis et al. (2018) and Hole et al. (2019) and quantifying the influence of these interactions on oil pathways.

Abbreviations

ADIOS	Automated Data Inquiry for Oil Spills
API	American Petroleum Institute gravity
CEEZ	Cuban Exclusive Economic Zone
ECMWF	European Center for Medium-Range Weather Forecasts
FC	Florida Current
(N)GoM	(Northern) Gulf of Mexico
GSHHS	Global Self-consistent, Hierarchical, High-resolution Shoreline Database
HYCOM	HYbrid Coordinate Ocean Model
LC	Loop Current
NOAA	National Oceanic and Atmospheric Administration
WFA	Western Florida Anticyclones

CRediT authorship contribution statement

VK: Conceptualization, Methodology, Writing- Reviewing and Editing
YA: Writing- Reviewing and Editing, Formal analysis, Visualization
VA: Software, Validation
KFD: Software, Validation
AC: Writing- Reviewing and Editing
HK: Writing- Reviewing and Editing, Software
MH: Writing- Reviewing and Editing
LRH: Original draft preparation, Writing- Reviewing and Editing, Formal analysis

Declaration of competing interest

The authors declare that they have no known competing financial interests or personal relationships that could have appeared to influence the work reported in this paper.

Acknowledgments

This research was made possible in part by a grant from The Gulf of Mexico Research Initiative (#G-231819) and in part by the National Academy of Sciences, Engineering and Medicine (Gulf Research Program UGOS #2000011056). Atmospheric and wave data were kindly provided by the European Center for Medium- Range Weather Forecasts (ECMWF). M. Le Hénaff received partial support by NOAA/AOML and was supported in part under the auspices of the Cooperative Institute for Marine and Atmospheric Studies (CIMAS), a cooperative institute of the University of Miami and NOAA (agreement NA10OAR4320143). Data are publicly available through the Gulf of Mexico Research Initiative Information & Data Cooperative (GRIIDC) at https://data.gulfresearchinitiative.org, (GRIIDC) - doi: https://doi.org/10.7266/ABJRN4QK.

Appendix A. Weber number and Ohnesorge number

The Weber number, We, is a dimensionless number describing the relative importance of inertial forces and oil–water interfacial tension. We is a function of the sea water density, ρ_w, the significant wave height, H_s, and the oil–water interfacial tension, σ_{o-w}, and is given by

$$\mathrm{We} = \frac{\rho_w g H_s d_o}{\sigma_{o-w}}, \tag{2}$$

where g is the acceleration of gravity and $d_o = 4\sqrt{\frac{\sigma_{o-w}}{g(\rho_w - \rho_o)}}$ is the Rayleigh–Taylor instability maximum diameter.

The Ohnesorge number, Oh, is a dimensionless number describing the ratio of viscous forces to inertial and surface tension forces. Oh is a function of the dynamic oil viscosity, μ_o, oil density, ρ_o, and oil–water interfacial tension:

$$\mathrm{Oh} = \frac{\mu_o}{\sqrt{(\rho_o \sigma_{o-w} d_o)}}. \tag{3}$$

References

Abascal, A.J., Castanedo, S., Minguez, R., Medina, R., Liu, Y., Weisberg, R.H., 2015. Stochastic Lagrangian trajectory modeling of surface drifters deployed during the Deepwater Horizon oil spill. In: Proceedings of the Thirty-eighth AMOP Technical Seminar; Environment Canada: Ottawa, ON, Canada, pp. 77–91.

Androulidakis, Y., Kourafalou, V., Özgökmen, T., Garcia-Pineda, O., Lund, B., Le Hénaff, M., Hu, C., Haus, B.K., Novelli, G., Guigand, C., et al., 2018. Influence of river-induced fronts on hydrocarbon transport: a multiplatform observational study. Journal of Geophysical Research: Oceans 123, 3259–3285.

Androulidakis, Y., Kourafalou, V., Le Hénaff, M., Kang, H., Sutton, T., Chen, S., Hu, C., Ntaganou, N., 2019. Offshore spreading of Mississippi waters: pathways and vertical structure under eddy influence. Journal of Geophysical Research: Oceans 124, 5952–5978.

Androulidakis, Y., Kourafalou, V., Le Hénaff, M., Kang, H., Ntaganou, N., Hu, C., 2020a. Gulf stream evolution through the straits of Florida: the role of eddies and upwelling near Cuba. Ocean Dynamics 1–28.

Androulidakis, Y., Kourafalou, V., Robert Hole, L., Le Hénaff, M., Kang, H., 2020b. Pathways of oil spills from potential Cuban offshore exploration: influence of ocean circulation. Journal of Marine Science and Engineering 8, 535.

Androulidakis, Y., Kourafalou, V., Le Hénaff, M., Kang, H., Ntaganou, N., 2021. The role of mesoscale dynamics over northwestern Cuba in the loop current evolution in 2010, during the Deepwater Horizon incident. Journal of Marine Science and Engineering 9, 188.

Bleck, R., 2002. An oceanic general circulation model framed in hybrid isopycnic-Cartesian coordinates. Ocean Model. 4, 55–88.

Breivik, Ø., Bidlot, J.-R., Janssen, P.A., 2016. A stokes drift approximation based on the Phillips spectrum. Ocean Model. 100, 49–56.

Brekke, C., Espeseth, M.M., Dagestad, K.-F., Röhrs, J., Hole, L.R., & Reigber, A. (2020). Integrated analysis of multisensor datasets and oil drift simulations-a free floating oil

experiment in the open ocean. Journal of Geophysical Research: Oceans, (p. e2020JC016499).
Dagestad, K.-F., Röhrs, J., 2019. Prediction of ocean surface trajectories using satellite derived vs. modeled ocean currents. Remote Sens. Environ. 223, 130–142.
Dagestad, K.-F., Röhrs, J., Breivik, Ø., Ådlandsvik, B., 2018. Opendrift v1. 0: a generic framework for trajectory modelling. Geosci. Model Dev. 11, 1405–1420.
Delvigne, G.A.L., Sweeney, C., 1988. Natural dispersion of oil. Oil and Chemical Pollution 4, 281–310.
Drouin, K.L., Mariano, A.J., Ryan, E.H., Laurindo, L.C., 2019. Lagrangian simulation of oil trajectories in the Florida Straits. Mar. Pollut. Bull. 140, 204–218.
ECMWF, 2020. European centre for medium-range weather forecasts. https://www.ecmwf.int/en/forecasts/accessing-forecasts. (Accessed 25 May 2020).
ECMWFwave (2020). Ecmwf wave forecasts. http://apps.ecmwf.int/mars-catalogue/?class=od_stream=wave. Accessed: 2020-05-25.
Ehard, B., Malardel, S., Dörnbrack, A., Kaifler, B., Kaifler, N., Wedi, N., 2016. Comparing ecmwf high resolution analyses to lidar temperature measurements in the middle atmosphere. Q. J. R. Meteorol. Soc. 144 (712), 633–640.
Genaw, J.L., 2010. A discussion of environmental policy. Ind. Int'l & Comp. L. Rev. 20, 47.
Group, T. W, 1988. The WAM model—a third generation ocean wave prediction model. J. Phys. Oceanogr. 18, 1775–1810.
Haiden, T., Janousek, M., Bidlot, J., Ferranti, L., Prates, F., Vitart, F., Bauer, P., Richardson, D., 2016. Evaluation of ECMWF Forecasts, Including the 2016 Resolution Upgrade (European Centre for Medium Range Weather Forecasts).
Hole, L.R., Dagestad, K.-F., Röhrs, J., Wettre, C., Kourafalou, V.H., Androulidakis, Y., Kang, H., Le Hénaff, M., Garcia-Pineda, O., 2019. The Deepwater Horizon oil slick: simulations of river front effects and oil droplet size distribution. Journal of Marine Science and Engineering 7, 329.
HYCOM, 2020. Hybrid coordinate ocean model. www.hycom.org. (Accessed 25 May 2020).
Ji, Z., Johnson, W., DuFore, C., 2016. Oil Spill Risk Analysis: Gulf of Mexico Outer Continental Shelf (OCS) Lease Sales, Eastern Planning Area, Central Planning Area and Western Planning Area, 2017–2021, and Gulfwide OCS Program, 2017–2086, 33. BOEM, Sterling, VA (OCS Report).
Johansen, Ø., Reed, M., Bodsberg, N.R., 2015. Natural dispersion revisited. Mar. Pollut. Bull. 93, 20–26.
Jones, C.E., Dagestad, K.-F., Breivik, Ø., Holt, B., Röhrs, J., Christensen, K.H., Espeseth, M., Brekke, C., Skrunes, S., 2016. Measurement and modeling of oil slick transport. Journal of Geophysical Research: Oceans 121, 7759–7775.
Kourafalou, V.H., Kang, H., 2012. Florida current meandering and evolution of cyclonic eddies along the Florida Keys reef tract: are they interconnected? Oceans, Journal of Geophysical Research, p. 117.
Kourafalou, V.H., Lee, T.N., Oey, L.-Y., Wang, J.D., 1996. The fate of river discharge on the continental shelf: 2. Transport of coastal low-salinity waters under realistic wind and tidal forcing. Journal of Geophysical Research: Oceans 101, 3435–3455.
Kourafalou, V., Androulidakis, Y., Le Hénaff, M., Kang, H., 2017. The dynamics of Cuba anticyclones (Cubans) and interaction with the loop current/Florida current system. Journal of Geophysical Research: Oceans 122, 7897–7923.
Kourafalou, V.H., Androulidakis, Y., Kang, H., Smith, R., Valle-Levinson, A., 2018. Physical connectivity between Pulley Ridge and Dry Tortugas coral reefs under the influence of the Loop Current/Florida Current system. Prog. Oceanogr. 165, 75–99.
Le Hénaff, M., Kourafalou, V.H., 2016. Mississippi waters reaching South Florida reefs under no flood conditions: synthesis of observing and modeling system findings. Ocean Dyn. 66, 435–459.
Le Hénaff, M., Kourafalou, V.H., Paris, C.B., Helgers, J., Aman, Z.M., Hogan, P.J., Srinivasan, A., 2012. Surface evolution of the Deepwater Horizon oil spill patch: combined effects of circulation and wind-induced drift. Environmental Science & Technology 46, 7267–7273.
Le Hénaff, M., Kourafalou, V., Androulidakis, Y., Smith, R., Kang, H., Hu, C., Lamkin, J., 2020. In situ measurements of circulation features influencing cross-shelf transport around Northwest Cuba (submitted). Journal of Geophysical Research: Oceans 125 (7).
Lehr, W., Jones, R., Evans, M., Simecek-Beatty, D., Overstreet, R., 2002. Revisions of the ADIOS oil spill model. Environ. Model Softw. 17, 189–197.
Li, C., Miller, J., Wang, J., Koley, S.S., Katz, J., 2017a. Size distribution and dispersion of droplets generated by impingement of breaking waves on oil slicks. Journal of Geophysical Research: Oceans 122, 7938–7957.
Li, Z., Spaulding, M., McCay, D.F., Crowley, D., Payne, J.R., 2017b. Development of a unified oil droplet size distribution model with application to surface breaking waves and subsea blowout releases considering dispersant effects. Mar. Pollut. Bull. 114, 247–257.
Li, Z., Spaulding, M.L., French-McCay, D., 2017c. An algorithm for modeling entrainment and naturally and chemically dispersed oil droplet size distribution under surface breaking wave conditions. Mar. Pollut. Bull. 119, 145–152.
Lindeman, K.C., Lee, T.N., Wilson, W., Claro, R., Ault, J.S., 2001. Transport of larvae originating in southwest Cuba and the Dry Tortugas: evidence for partial retention in grunts and snappers. In: Proceedings of the Gulf and Caribbean Fisheries Institute, volume 5. Gulf and Caribbean Fisheries Institute, p. 1.
Liu, Y., MacFadyen, A., Ji, Z.-G., Weisberg, R.H., 2011. Monitoring and Modeling the Deepwater Horizon Oil Spill: A Record Breaking Enterprise volume 195. AGU/geopress.
Murawski, S.A., Ainsworth, C.H., Gilbert, S., Hollander, D.J., Paris, C.B., Schlüter, M., Wetzel, D.L., 2019. Scenarios and Responses to Future Deep Oil Spills: Fighting the Next War. Springer.
NOAA-Oil (2020). NOAA - oil library. github.com/NOAA-ORR-ERD/OilLibrary. Accessed: 2021-02-25.
Nordam, T., Kristiansen, R., Nepstad, R., Rhrs, J., 2019. Numerical analysis of boundary conditions in a Lagrangian particle model for vertical mixing, transport and surfacing of buoyant particles in the water column. Ocean Model. 136, 107–119.
Oey, L., Ezer, T., Lee, H., 2005. Loop current, rings and related circulation in the Gulf of Mexico: a review of numerical models and future challenges. Geophysical Monograph-American Geophysical Union 161, 31.
oildrift, N. (2019). NOAA oil drift model. github.com/NOAA-ORR-ERD/PyGnome. Accessed: 2021-02-25.
OpenDrift, 2020. Opendrift - open source framework for ocean trajectory modelling. www.github.com/opendrift. (Accessed 25 February 2021).
Pérez-Santos, I., Schneider, W., Fernández-Vila, L., 2015. Features and variability of the Cuban Countercurrent in the Yucatan Basin, Caribbean Sea. Ciencias Marinas 41, 65–83.
Röhrs, J., Dagestad, K.-F., Asbjørnsen, H., Nordam, T., Skancke, J., Jones, C., Brekke, C., 2018. The effect of vertical mixing on the horizontal drift of oil spills. Ocean Science Discussions 14 (6), 1581–1601.
Schiller, R.V., Kourafalou, V.H., 2010. Modeling river plume dynamics with the hybrid coordinate ocean model. Ocean Model. 33, 101–117.
Schwartzberg, H.G., 1971. The movement of oil spills. In: International Oil Spill Conference. American Petroleum Institute, pp. 489–494.
Sturges, W., Evans, J., 1983. On the variability of the loop current in the Gulf of Mexico. J. Mar. Res. 41, 639–653.
Sundby, S., 1983. A one-dimensional model for the vertical distribution of pelagic fish eggs in the mixed layer. Deep Sea Research Part A. Oceanographic Research Papers 30, 645–661.
Tkalich, P., Chan, E.S., 2002. Vertical mixing of oil droplets by breaking waves. Mar. Pollut. Bull. 44, 1219–1229.
Visser, A.W., 1997. Using random walk models to simulate the vertical distribution of particles in a turbulent water column. Mar. Ecol. Prog. Ser. 158, 275–281.
Weisberg, R.H., Lianyuan, Z., Liu, Y., 2017. On the movement of Deepwater Horizon oil to northern gulf beaches. Ocean Model. 111, 81–97.